Comparison of Observed 10-m Wind Speeds to Those Based on Monin–Obukhov Similarity Theory Using IHOP_2002 Aircraft and Surface Data

DIANE STRASSBERG

National Center for Atmospheric Research, and Department of Atmospheric and Oceanic Sciences, University of Colorado, Boulder, Colorado

MARGARET A. LEMONE

National Center for Atmospheric Research, Boulder, Colorado

THOMAS T. WARNER

National Center for Atmospheric Research, and Department of Atmospheric and Oceanic Sciences, University of Colorado, Boulder, Colorado

JOSEPH G. ALFIERI

Department of Agronomy, Purdue University, West Lafayette, Indiana

(Manuscript received 19 March 2007, in final form 25 May 2007)

ABSTRACT

Comparisons of 10-m above ground level (AGL) wind speeds from numerical weather prediction (NWP) models to point observations consistently show that model daytime wind speeds are slow compared to observations, even after improving model physics and going to smaller grid spacing. Previous authors have attributed the discrepancy to differences between the areas represented by model and observations, and the small surface roughness upstream of wind vanes compared with the corresponding model grid value. Using daytime fair-weather data from the May–June 2002 International H_2O Experiment (IHOP_2002), the effect of wind-vane exposure is explored by comparing observed 10-m winds from nine surface-flux towers in well-exposed locations to modeled 10-m winds found by applying Monin–Obukhov (MO) similarity for unstable conditions to flight-track-averaged data collected by the University of Wyoming King Air over flat to rolling terrain with occasional trees and buildings. In the calculations, King Air winds and fluxes are supplemented with thermodynamic means and fluxes from the surface-flux towers. After exercising considerable care in characterizing and reducing biases in aircraft winds and fluxes, the authors found that MO-based surface winds averaged 0.5–0.7 $\pm$ 0.2 m s^{-1} less than those measured—about the same as the smaller reported discrepancies between NWP models and observed winds.

1. Introduction

Numerous studies show that daytime fair-weather surface wind speeds predicted by numerical weather prediction (NWP) models tend to be slower than observed wind speeds. Applying five different planetary boundary layer (PBL) schemes in the fifth-generation Pennsylvania State University–National Center for Atmospheric Research (PSU–NCAR) Mesoscale Model (MM5) to simulate the diurnal cycle of wind and temperature under weakly forced fair-weather conditions, Zhang and Zheng (2004) found that the daytime model winds were consistently 0.5–2.0 m s^{-1} weaker than those observed. Even after improving the boundary layer parameterization scheme, Liu et al. (2006) found that daytime winds produced by MM5 still averaged ~0.5 m s^{-1} lower than measured surface winds around Oklahoma City, Oklahoma.

Aside from shortcomings in NWP model physics, two explanations are given for discrepancies between mod-

Corresponding author address: Margaret A. LeMone, NCAR Foothills Laboratory, 3450 Mitchell Lane, Boulder, CO 80301.
E-mail: lemone@ucar.edu

DOI: 10.1175/2007MWR2203.1

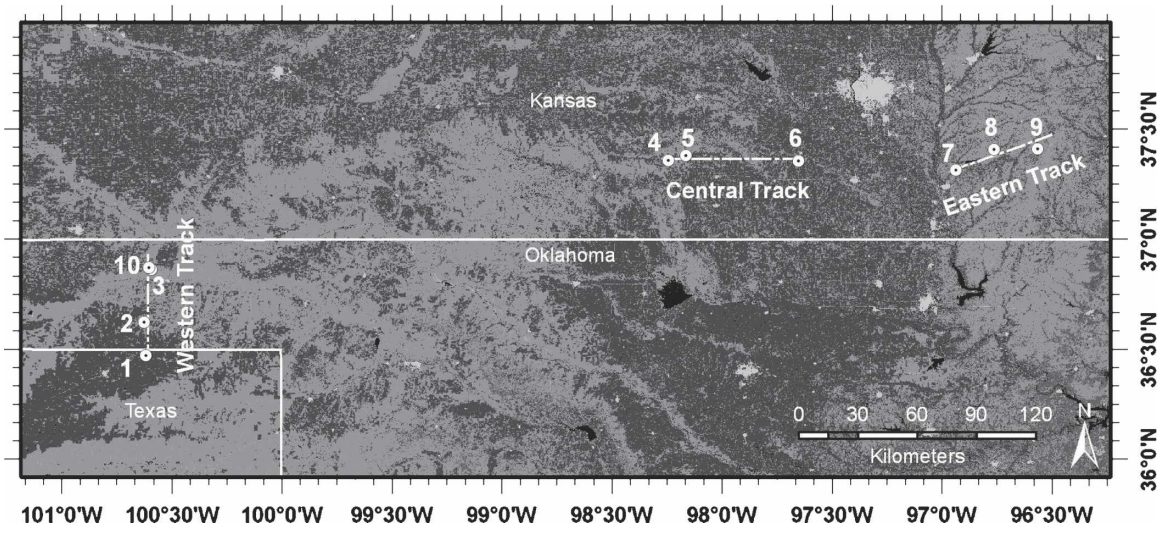

FIG. 1. Location of the western, central, and eastern tracks with associated surface-flux sites (numbered 1–10), superimposed on a map of land-use types: open water (dark shading), winter wheat (dark gray shading), and grasslands (lighter shading).

eled and observed surface winds: the much greater area represented by a model grid area compared to a "point" measurement (which could lead to a discrepancy of either sign); and observations being taken in open areas with less effective roughness than the model grid average, which includes the effects of complex terrain, as well as trees and buildings (which should lead to model winds being slower than observed winds). Rife et al. (2004) summarize several previous studies of NWP model success in predicting surface variables in terrain of varying complexity, noting that reduction of grid size improved results down to about 10 km, but further reduction did not necessarily mean an improvement in forecast success. Their own 1.33-km-grid-size MM5 simulations of the flow in the Salt Lake City, Utah, area performed only slightly better than comparable models run on 30- and 40-km grids. They attributed some of the remaining discrepancy to still-unresolved effects at the smallest scales. De Rooy and Kok (2004) discussed the point measurement problem and dealt with it in a mesoscale model by developing a method to downscale surface winds using local roughness lengths.

We explore the daytime model–observation discrepancy associated with using point measurements by comparing surface winds observed at well-exposed locations to surface winds calculated by applying Monin–Obukhov (MO) similarity theory to aircraft data averaged along 50–60-km flight tracks, supplemented with thermodynamic data from nearby surface-flux towers (Fig. 1). The data were collected in the convective boundary layer over the Southern Great Plains of Kansas, Oklahoma, and Texas on fair-weather days during the May–June 2002 International H_2O Experiment (IHOP_2002; Weckwerth et al. 2004; LeMone et al. 2007a). The surface-flux towers were sited in open areas along the three King Air flight tracks to provide representative samples of fluxes over the dominant surface-cover types (grassland, winter wheat, bare ground, sagebrush), while the aircraft data included the effects of trees, buildings, and terrain as well as the shallow vegetation. Given that the surface winds were measured over shallow vegetation, we expect them to be stronger than those calculated from MO similarity theory.

After outlining the data requirements using the theoretical background in section 2, we discuss data collection and processing in section 3. Section 4 outlines the data-analysis procedure, the random and bias errors, and removal of biases. Results are presented and discussed in section 5, with conclusions in section 6.

2. Theory

Surface wind speeds are calculated from MO similarity theory, following Paulson (1970). Thus the wind speed S_h at a height z_h is given by

$$S_h = \frac{u_*}{k}\left[\ln\left(\frac{z_h}{z_0}\right) - \Psi_h\right], \tag{1}$$

where z_0, the effective roughness length for the area sampled along the flight track, includes the effects of buildings, trees, and terrain, as well as grassland and crops. For unstable conditions, the stability correction Ψ_h at z_h is given by

TABLE 1. Characteristics of the days used in the analysis. Values interpolated to 1830 UTC (local solar noon). W = western track, E = eastern track, and C = central track.

Date	Track	On-station times (UTC)	Legs at 65 m AGL	BL depth (m)	z_{ac} (m AGL)	$U(z_{ac})$ (m s^{-1})	$V(z_{ac})$ (m s^{-1})
29 May	W	1640:07–2024:05	5	1030	62.0	1.14	4.72
30 May	E	1644:04–1951:06	8	900	67.4	−1.30	3.42
31 May	C	1744:45–2035:00	7	1450	63.9	0.99	6.47
7 Jun	W	1650:37–1958:59	7	1000	62.0	2.71	9.73
17 Jun	E	1647:40–2020:13	6	1240	67.8	2.74	7.01
20 Jun	E	1641:43–2036:08	5	1250	64.2	−1.55	4.83
22 Jun	E	1708:15–2115:40	10	1260	62.7	−0.30	9.67

$$\Psi_h = 2\ln\left(\frac{1+x}{2}\right) + \ln\left(\frac{1+x^2}{2}\right) - 2\tan^{-1}x + \frac{\pi}{2}, \tag{2}$$

where $x = (1 - 16z/L)^{1/4}$, and the Obukhov length $L = -(u_*^3\overline{T_v})/(kg\overline{w'T_v'})$, where u_* is the friction velocity, $\overline{T_v}$ is a reference temperature, taken here as the average virtual temperature, k is the von Kármán constant (taken as 0.4), g is the acceleration due to gravity, and $\overline{w'T_v'}$ is the vertical eddy flux of virtual temperature.

Rewriting (1) for the aircraft height [$z_{ac} \sim 65$ m above ground level (AGL)] and the surface observation height ($z_{10} = 10$ m AGL), we solve for the effective 10-m wind speed S_{10} by subtracting S_{ac} from S_{10} and rearranging:

$$S_{10} = S_{ac} - \left(\frac{u_*}{k}\right)\left[\ln\left(\frac{z_{ac}}{z_{10}}\right) - \Psi_{ac} + \Psi_{10}\right]. \tag{3}$$

Being associated with the effective roughness length for the entire flight track, S_{10} is interpreted as the analog to an NWP-model 10-m wind for a comparable grid area.

For MO similarity to apply, z_{ac} and z_{10} should lie within the surface layer. Physically, the surface layer is defined as that layer through which shear generates more turbulence than buoyancy (Glickman 2000). Since the Obukhov length is a ratio of shear to buoyancy effects, it follows that MO stability applies for $-(z/L) < 1$; in the Kansas-experiment surface-layer data of Businger et al. (1971), data fit the MO similarity curves out to $-z/L \sim 1.5$, with a few points to 2.2. According to Wyngaard (1983) and Brutsaert (1998), the surface layer extends to ~10% of the PBL depth. However, the definition can be more conservative than this: Mahrt (2000) uses 5% of the convective boundary layer depth as the upper limit for the surface-layer top, and the American Meteorological Society (AMS) *Glossary of Meteorology* (Glickman 2000) definition extends the surface layer up to a few tens of meters. Here, we require that $z_{ac} < 0.1z_i$ and look at data for both $z_{ac} < -L$ and $z_{ac} < -1.5L$.

Wood and Mason (1991), Mahrt (2000), and others also require that the measurements be above the "blending height" for MO similarity to apply. We use Wood and Mason's Eq. (4), which defines the blending height l_b as that height above which the horizontally averaged mean flow can be expected to assume an MO type profile [(1)] with an effective roughness length z_0 that is independent of height. Thus z_{10} must satisfy

$$z_{10} > l_b \sim \frac{\lambda}{\pi}\left(\frac{u_*}{S_{10}}\right)^2, \tag{4}$$

where λ is the characteristic scale of horizontal heterogeneity. The blending height l_b is not to be confused with Wood and Mason's diffusion height, a higher altitude at which horizontal variations related to surface heterogeneity disappear. Thus such variations can occur, but their effect on the mean wind averages to zero. Since (4) worked well for a large eddy simulation with $L \sim -76$ m in Wood and Mason, it should be reasonable for at least a subset of the IHOP_2002 data.

3. Data collection and processing

Measurements used for our analysis were collected during IHOP_2002 from the University of Wyoming King Air aircraft and NCAR surface-flux towers. The aircraft data are from the boundary layer heterogeneity (BLH) missions (Table 1), flown during fair weather, along the western, central, or eastern tracks, shown in Fig. 1. In Table 1, the mean winds U and V are in a right-handed coordinate system with U pointing east.

The most relevant aircraft measurements are summarized in Table 2. The winds were calculated by subtracting the velocity of the aircraft relative to the earth from the velocity of the air relative to the aircraft. The aircraft-relative wind was measured by the differential pressure gust-probe system, while the ground-relative motion and position were measured by the inertial navigation system and corrected using GPS data. Data were recorded at 25 Hz.

TABLE 2. Applicable measurements from University of Wyoming King Air.

Measurement	Sensor
Pressure	Rosemount 1201 (pmb)
Altitude	King Air APN 159 radar altimeter (ralt2)
	King KRA5 radio altimeter (ralt1, heights below 610 m)
Temperature	In-house (University of Wyoming) reverse-flow thermometer (thetad)
Wind	Aircraft-relative motion from a Rosemount 858AJ/1332 differential pressure gust-probe system
	Ground-relative motion and position from a Honeywell Laseref SM inertial navigation system (with GPS corrections, hu, hv, hw)
Mixing ratio	Li-Cor 6262 gas analyzer (h2omx)

On a given day, the King Air flew 10 to 18 straight-and-level 50–60-km legs over one track at two or more levels within the boundary layer, from ~65 m AGL to just over 1000 m AGL, interspersed with vertical soundings to determine PBL depth. These data were collected in fair weather during 4-h flights centered around local noon (~1830 UTC), to sample the PBL after its most rapid growth but when it is still strongly coupled to the surface. For this analysis, only days with five or more legs at ~65 m AGL were used. The seven days satisfying this requirement are 29, 30, and 31 May and 7, 17, 20, and 22 June (Table 1).

The surface data came from nine surface-flux towers operated by NCAR (numbered 1–9 in Fig. 1). Stations 1–3 were along the western track, 4–6 along the central track, and 7–9 along the eastern track. The fourth site (station 10) along the western track was not included since it did not collect all of the data necessary for this analysis and the winds were not measured at 10 m AGL. The stations were located to sample the major land-use types—grassland, winter wheat, bare ground, and sagebrush—along the three tracks. In addition to scattered buildings, there are trees along all three tracks, mainly located along rivers or bordering fields.

Relevant surface measurements are summarized in Table 3. We used half-hour data, available from www.rap.ucar.edu/research/land/observations/ihop.php. Sensible heat flux H and latent heat flux LE were computed relative to half-hour averages, using 5-min block averages that were quality-checked and postprocessed by the Integrated Surface Flux Facilities (ISFF) of NCAR using a standard suite of corrections that are summarized at http://www.eol.ucar.edu/rtf/projects/ihop_2002/isff/. The water vapor flux was estimated from the water vapor concentration and sonic anemometer vertical velocity. The temperature flux was calculated from the vertical sonic-temperature flux using the specific humidity flux in the standard way (Schotanus et al. 1983). Half-hour averaged temperature, mixing ratio, and pressure were used to convert the temperature and water vapor fluxes to H and LE. Because of problems with some of the water vapor sensors, we used the LE values found as a residual from the surface energy balance. The resulting surface fluxes were within 10%–15% of the aircraft fluxes extrapolated to the surface (LeMone et al. 2007a).

4. Data analysis

In (3), we use wind speed and momentum fluxes (from aircraft), virtual-temperature fluxes (from surface and aircraft), and virtual temperature (from surface and aircraft) to obtain S_{10}. Ideally, we would use aircraft data only. However, we use surface thermodynamic fluxes to offset the typical biases between aircraft and surface data (e.g., Desjardins et al. 1992; Betts et al. 1992), and we use surface thermodynamic data to get a better average virtual temperature for use in calculating L. Only the aircraft legs at ~65 m AGL are used for

TABLE 3. Applicable measurements from surface stations.

Measurement	Parameter	Height (m AGL)	Sensor
Wind speed and direction	u_{10}	10	RM Young 9101 Prop Vane Anemometer
H_2O vapor concentration	L, H, LE	2–3	Campbell Scientific KH2O Krypton Hygrometer
Temperature	L, H, LE	2–3	Vaisala 50Y Hummitter
Air pressure	H, LE	—	Vaisala PTB220B
Mixing ratio	L, H, LE	2–3	Vailsala 50Y Hummitter (measured as relative humidity, converted to mixing ratio during post processing)
Sonic wind speed and temperature (sites 1, 2, 3, 4, 7)	H, LE	2–3	Campbell Scientific CSAT3 Sonic Anemometer
Sonic wind speed and temperature (sites 5, 6, 8, 9)	H, LE	2–3	Applied Technologies, Inc., Sonic Anemometer

momentum-flux estimates. With typically more legs flown (a larger sample) and a smaller turbulence integral scale (and hence effectively more eddies sampled per leg) than at higher altitudes, the fluxes at ~65 m have the least uncertainty. To mitigate the effects of time trends, all surface and aircraft fluxes and variables are computed so that their values apply to 1830 UTC.

a. Aircraft data

1) FLUX CALCULATION

The temperature flux ($\overline{w'T'}$), water vapor flux ($\overline{w'q'}$), and the components of the momentum flux ($\overline{u'w'}$ and $\overline{v'w'}$) for each flight leg were calculated as covariances, after shifting the T and q time series to account for horizontal separation on the aircraft and differences in time response of the thermodynamic sensors relative to the vertical-velocity sensors, as described in LeMone et al. (2007b). The primes are defined relative to the flight-leg linear trend, and the overbars indicate flight-leg averages.

A heading-related bias in both wind speed and momentum fluxes results from true airspeed and side-slip angle biases. For example, when the aircraft was flying south-to-north along the western track, the along-aircraft bias (due to true-airspeed bias) influenced V and $\overline{v'w'}$, while the cross-aircraft bias (due to side-slip angle bias) influenced U and $\overline{u'w'}$.

To calculate and remove the aircraft biases for the wind and momentum fluxes, plots were made for both fluxes as a function of time to compare values for opposing aircraft headings, and the data was fitted to straight lines using a least squares best-fit linear regression. Half the difference between the opposite-heading values at a common time (ideally the center time for both plots) was taken as the bias. Were the flight legs with opposite headings equal in number and evenly distributed through time, such a step would not be necessary. Typical momentum-flux biases were of the order of 0.1 $m^2 s^{-2}$ parallel to the aircraft and about 0.01 $m^2 s^{-2}$ normal to the aircraft; while typical wind speed biases were a few tenths of a meter per second.

Once the biases were removed, the wind and momentum fluxes at each height interval were replotted as a function of time, and their values at 1830 UTC found using least squares best-fit straight lines. The 1830 UTC surface momentum fluxes were found assuming that the total flux fell along a straight line with a value of zero at the boundary layer top z_i (Table 1), following a profile similar to that produced for the vertical flux of the along-wind component in large-eddy simulations (e.g., Moeng and Sullivan 1994). For small shear at the PBL top, the expected curvature of the relatively small vertical flux of the horizontal wind component normal to the mean PBL wind should not introduce significant error, since the momentum-flux correction is through a depth small (30–50 m) compared to z_i, (~1000 m); that is, any error would be a fraction of the ~3%–5% correction. However, for days with large vertical shear of the horizontal wind near z_i, large eddy simulations by Conzemius and Fedorovich (2006) show that vertical flux of the lateral wind component can have significant curvature and thus potentially lead to significant error in the downward extrapolation. We looked for "large-shear" cases both by examining aircraft soundings and by testing to see whether the entrainment ratio

$$A = -\frac{(\overline{w'T'_v})_{z_i}}{(\overline{w'T'_v})_{\mathrm{sfc}}} \tag{5}$$

was greater than 0.2, the value associated with small shear at z_i.

For temperature and water vapor fluxes, the aircraft data were treated similarly. However, the surface values were based on the surface-station measurements.

2) SOURCES OF ERROR FOR AIRCRAFT WIND AND MOMENTUM FLUX

The mean wind estimate S_{ac}, and hence S_{10} in (3), is affected by ground speed error $\varepsilon_{S_{10}}(S_{\mathrm{ac,gs}})$ and a random error aircraft-relative wind from turbulent fluctuations $\varepsilon_{S_{10}}(S_{\mathrm{ac},r})$. We can estimate $\varepsilon_{S_{10}}(S_{\mathrm{ac,gs}})$ from the King Air position uncertainty, which was ~0.1 km during IHOP_2002 (A. Rodi 2005, personal communication). Thus the fractional error in distance traveled for a 50-km flight leg due to position error is 0.2 km/50 km or 0.004. For a ground speed of 80 m s^{-1}, this translates to a 0.3 m s^{-1} uncertainty in ground speed for a single flight leg, or a standard error of 0.14 m s^{-1} for a five-leg average.

The random error $\varepsilon_{S_{10}}(S_{\mathrm{ac},r})$ is related to the magnitude of the turbulence and the scale of the eddies relative to the distance sampled. For a single flight leg, the u component, ε_U, of $\varepsilon_{S_{10}}(S_{\mathrm{ac},r})$ is found from

$$\varepsilon_U = \sqrt{\frac{2\lambda_u}{L_x}}\,\sigma_u, \tag{6}$$

where λ_u is the integral scale for u, L_x is the mean length of the flight track, and σ_u is the standard deviation (Wyngaard 1983). The error for all the flight legs is then found from

$$\varepsilon_{N_{\mathrm{legs}}} = \left(\sum_{i=1}^{N_{\mathrm{legs}}} \frac{1}{\varepsilon_i^2}\right)^{-1/2}, \tag{7}$$

where $\varepsilon_i = \varepsilon_U$ for the ith leg. A similar procedure is used to find ε_V. The errors for the two wind components were combined vectorially to obtain $\varepsilon_{S_{10}}(S_{\mathrm{ac},r})$. Values range from 0.09 to 0.17 m s^{-1}.

The random uncertainty for u_*, $\varepsilon_{u_*(r)}$, contributes to $\varepsilon_{S_{10}(u_*,r)}$ the uncertainty in S_{10} through (3). We calculated $\varepsilon_{u_*(r)}$ from the random error in the momentum fluxes, which is found for a single flight leg, from

$$\sigma(\overline{w'c'}) = \left(\frac{2\lambda_F}{L_x}\right)^{1/2}\left(\frac{1 + r^2_{w',c'}}{r^2_{w',c'}}\right)^{1/2}\overline{w'c'} \qquad (8)$$

(Mann and Lenschow 1994), where $r^2_{w,c}$ is the correlation coefficient between w' and c' ($=u'$ or v'); λ_F is the flux integral scale, which was found from the peaks of the frequency-weighted spectra for the products $u'w'$ and $v'w'$ (following Lenschow 1995); and L_x is the flight-leg length. The uncertainty $\sigma_{N_{\mathrm{legs}}}(\overline{w'c'})$ for all flight legs (N_{legs}) was calculated from (7) with $\varepsilon_i = \sigma(\overline{w'c'})$ for the ith flight leg and $\varepsilon_{N_{\mathrm{legs}}} = \sigma_{N_{\mathrm{legs}}}(\overline{w'c'})$.

To find $\varepsilon_{S_{10}(u_*,r)}$, the uncertainty $\varepsilon_{u_*(r)}$ was found by adding/subtracting $\sigma_{N_{\mathrm{legs}}}(\overline{w'c'})$ from the corresponding average momentum flux component, finding the total stress for the various mean-error combinations, converting the largest and smallest stress values to the largest and smallest u_*, and finally taking the difference to find $\varepsilon_{u_*(r)} = 0.5\ u_*$. These values were then used to modify u_* in $-L$ and (3) to determine the effect on S_{10}. Values of $\varepsilon_{S_{10}(u_*,r)}$ range from 0.06 to 0.16 m s^{-1}.

b. Surface data

1) Calculating surface values

For each day, the surface wind, virtual temperature, and virtual temperature fluxes were derived from half-hour averaged data for the three surface-flux sites along the track the King Air flew. The virtual temperature flux was derived from sensible heat flux H and latent heat flux LE, using corresponding values of pressure (P), temperature (T), and mixing ratio (Q). The 1830 UTC values for the track were found by averaging the values at 1815 and 1845 UTC at each site, and then averaging the result for all three sites.

2) Error in measured surface winds

The random error in the observed 10-m wind speed measurement $\varepsilon_{S_{10},\mathrm{obs}(r)}$ was found from averaging two estimates. The first estimate was based on (7), with the six individual flux-site half-hour values (three stations, two values) from empirical relationships (1.47) and (1.50) in Kaimal and Finnigan (1994). The aircraft integral scale for v was used for days when the wind was out of the south; the average of the integral scales for v and u was used for 30 May, when the wind was out of the SSE. Such estimates were necessary because only mean winds were recorded at 10 m. For the second estimate, we simply computed the standard error for the six 30-min averages used to estimate u_{10}. The resulting estimates vary between 0.1 and 0.2 m s^{-1}.

Instrument error for the surface wind is negligible. From Brock and Richardson (2001), the measurement error from propeller vanes varies as the cosine of the angle of the wind to the propeller; that is, the error comes from the vertical velocity (w). Using Eq. (13) of Lenschow et al. (1980) to estimate w, we found the contribution to be small. Since care is taken to ensure the flux towers are vertical, error due to departure from true vertical is also small.

c. Combined surface and aircraft data: Uncertainty in (3) from buoyancy-flux uncertainty

From the foregoing, aircraft and surface thermodynamic fluxes differed slightly, and LE was found as a residual from the surface energy budget. The uncertainty in buoyancy flux $\varepsilon_{S_{10}(B)}$ contributes to $\varepsilon_{S_{10}}$ through modifying $-L$ and thus to the stability corrections Ψ_{ac} and Ψ_{10} in (3). We estimate $\varepsilon_{S_{10}(B)}$ by allowing the buoyancy fluxes to differ by $\pm 7.5\%$ relative to the mean (roughly the difference between aircraft and surface data) to obtain the associated range of S_{10}. As for $\varepsilon_{S_{10}}(u_*, r)$, the error is set to half the range of extreme values, namely, $\varepsilon_{S_{10}(B)} = 0.5[S_{10}(1.075B) - S_{10}(0.925B)]$. The resulting values vary between 0.02 and 0.06 m s^{-1}.

d. Total estimated random error in S_{10} (calculated) − S_{10} (observed)

The total contribution of random measurement errors to the difference between S_{10} observed ($S_{10,\mathrm{obs}}$) and S_{10} calculated from (3) is therefore found from

$$\varepsilon_{S_{10(3)} - S_{10,\mathrm{obs}}} = [\varepsilon^2_{S_{10}(S_{\mathrm{ac,gs}})} + \varepsilon^2_{S_{10}(S_{\mathrm{ac},r})} + \varepsilon^2_{S_{10}(u_*,r)} + \varepsilon^2_{S_{10},\mathrm{obs}(r)} + \varepsilon^2_{S_{10}(B)}]^{1/2}, \qquad (9)$$

where the first three terms represent the aircraft data, the fourth term represents the observed surface wind, and the final term combines the contribution of the buoyancy-flux uncertainty from both aircraft and surface data.

Some sources of uncertainty are not accounted for, namely, the effects of aircraft flow distortion on the wind and momentum flux measurements (unknown but assumed to be small) and the effect of ground-speed error on momentum fluxes (assumed to be small). Further, the choice to use a best-fit linear trend to obtain

TABLE 4. Comparison of measured 10-m wind speeds to those predicted from (3) using averages from either 10 or 65 m (see text). Days in italics are not used; the remainder are considered satisfactory. Boldface days match shear and surface-layer criteria well and are designated good. W = western track, E = eastern track, and C = central track.

Date	Track	$S_{10,\mathrm{obs}}$ (m s^{-1})	S_{10} [(3)]; 10 m (m s^{-1})	S_{10} [(3)]; 65 m (m s^{-1})	S_{10} [(10)] $(z - d)$, d = 0.9 m; 65 m (m s^{-1})	$\pm\varepsilon_{\mathrm{random}}$ (7) (m s^{-1})	$-L_{10}/-L_{65}$ (m)	z_i (m)	l_b from (4) (m)	Significant shear at z_i?	$-\dfrac{(\overline{w'T'_v})_{z_i}}{(\overline{w'T'_v})_{\mathrm{sfc}}} > 0.2$
29 May	*W*	*4.28*	*4.02*	*4.02*	*3.97*	*0.33*	*24.9/26.3*	*1030*	*3.8*	*Yes*	*No*
30 May	*E*	*3.03*	*2.94*	*2.95*	*2.91*	*0.23*	*21.1/20.5*	*900*	*5.7*	*No*	*No*
31 May	C	5.51	5.27	5.23	5.16	*0.28*	44.7/53.7	1450	4.0	Yes	Yes
7 Jun	*W*	*8.51*	*8.42*	*8.41*	*8.32*	*0.25*	*71.2/78.4*	*1000*	*2.4*	*Yes*	*Yes*
17 Jun	**E**	**6.51**	**5.62**	**5.67**	**5.57**	**0.32**	**117/110**	**1240**	**4.1**	**No**	**No**
20 Jun	E	4.60	4.03	4.03	3.98	*0.23*	45.6/47.8	1250	3.8	No	No
22 Jun	**E**	**7.75**	**7.30**	**7.34**	**7.22**	**0.26**	**218/207**	**1260**	**3.9**	**No**	**No**

flux and wind values at a common time eliminates the effect of an asymmetric time distribution of flight legs, but adds uncertainty related to the linear fit. An additional source of uncertainty is that we have to assume that the source regions for the aircraft wind and momentum-flux measurements are sufficiently uniform in a statistical sense that (3) applies. Similarly, the aircraft source regions for a given flight track are assumed similar to the broader environment of the corresponding set of surface sites. That is, differences in the regional "footprints" for wind and momentum flux do not matter. Finally, we assume that the smaller footprints of the surface sites are representative of open areas in the region.

5. Results and discussion

The 10-m wind speeds estimated from (3) are compared to those observed at nearby surface-flux stations for each day in Table 4. The estimates labeled "10 m" are based on L and u_* calculated from averages at 10 m, while the estimates labeled "65 m" are calculated from the average of values at ~65 and 10 m.

From the foregoing, (3) applies provided that both z_{10} and z_{ac} are within the surface layer. Whether z_{ac} is below the surface-layer top depends on the definition; however, $z_{10} > l_b$ and hence within the lower part of the surface layer for all seven days according to (4). From the table, $z_{\mathrm{ac}} < 0.1z_{\mathrm{i}}$ for all the days. If we define the surface layer as extending up to $-1.5L$, the last five days fit this criterion for (3) to apply. Only 7, 17, and 22 June fit the $z_{\mathrm{ac}} < -L$ criterion. Using the size of a section of land (1.6 km) in (4), the blending height is always less than 10 m, implying that (3) applies, provided that the most significant horizontal heterogeneity is at that scale or less. This is not an unreasonable assumption, since crop areas are typically less than a section in size. If we invert (4) and solve for λ, the horizontal scales corresponding to l_b = 10 m vary from 2.8 km on 30 May to 6.6 km on 7 June. However, while (4) holds for $-L > 76$ m in Wood and Mason (1991), it could be argued that a blending-height estimate should involve w_* for more convective conditions.

Applying the vertical shear criteria of section 4a (Table 4, last two columns) to the five cases fitting the more generous definition of surface layer reduces the number of satisfactory cases to four—17, 20, and 22 June, with 31 May included simply because the momentum-flux height correction is so small. The shear criteria and the stricter $z_{\mathrm{ac}} < -L$ criterion are all met on both 17 and 22 June, so these are designated good cases. The aircraft soundings reveal significant shear at z_i for 31 May and 7 June [~1.3 m s^{-1} (100 m)$^{-1}$], and moderate shear on 29 and 30 May [~0.4–0.6 m s^{-1} (100 m)$^{-1}$], with values ~0.3 m s^{-1} (100 m)$^{-1}$ or less on 17, 20, and 22 June. To check this assessment, which is influenced by aircraft heading–dependent wind bias, we also estimated the entrainment ratio (5) assuming H and LE varied linearly with height, and found values <0.2 except for 31 May, when A was slightly larger than 0.2, and 7 June, when A was significantly larger than 0.2. However, we retained 31 May as marginally satisfactory since the magnitude of the momentum flux downward extrapolation is inversely proportional to z_i, which was 1450 m.

In Table 4, the observed wind exceeds the predicted wind by 0.5–0.6 ± 0.2 m s^{-1}, regardless of the qualifying days counted, or the averaging procedure to find L and u_*. For the four "satisfactory" days, the mean measured wind is 6.09 m s^{-1}, greater than the predicted speed for a 10- or 65-m constant flux layer (5.56 m s^{-1}), with a difference of 0.53 ± 0.13 m s^{-1}, with the uncertainty from (7). If we count only the two "good" days, the two values are 7.13 and 6.48 m s^{-1} (average of 6.46 and 6.51 m s^{-1}), respectively, yielding an average difference of 0.65 ± 0.20 m s^{-1}. Using flight-level momentum flux

instead of extrapolating to the surface reveals similar differences: 0.5 and 0.6 m s^{-1} for the satisfactory and good cases, respectively. These differences are about the same as the smallest discrepancies in Liu et al. (2006) and Zhang and Zheng (2004).

Often (1) and (3) are written with $z - d$ instead of z, where d is the displacement height, so that

$$S_{h(\mathrm{ac})} = \frac{u_*}{k} \ln\left(\frac{z_{h(\mathrm{ac})} - d}{z_0} - \Psi_{h(\mathrm{ac})}\right). \qquad (10)$$

To find d, we combine two commonly used relationships (e.g., Campbell and Norman 1998), $z_0 \sim 0.1h_c$ and $d \sim (2/3)h_c$, where h_c is the effective height of the canopy (buildings, trees, etc.), to obtain the relationship $d = 6.67z_0$. Substituting this into (10) and using the aircraft data for 22 June, we obtain a value of $d \sim 0.9$ m. From Table 4, using (10) instead of (3) increases the difference between observed and predicted S_{10} to ~0.61 m s^{-1} for the satisfactory cases and 0.74 m s^{-1} for the good cases.

Consistent with the reduced winds, the effective roughness length based on aircraft wind and momentum-flux data is larger than that for the surface sites. Applying either (3) or (10) to the data for 22 June, the effective roughness length for the eastern track was ~0.14 m. For comparison Stull (2000) lists $z_0 = 0.25$ m for high crops with occasional trees and hedgerows, and 0.1 m for low crops with occasional bushes. In contrast, z_0 at the three corresponding surface-flux sites (all grassland) was between 0.012 and 0.023 m, which are fairly typical values for grassland.

These results are consistent with those of Kustas et al. (2005), who found that u_* and z_0 from aircraft were larger than values based on surface data over corn and soybeans. They attributed the difference to form drag from isolated obstacles such as buildings and trees and the borders between different crops. Such obstacles do not have to be very big or cover a very large area to have a significant effect. For example, Hasager et al. (2003) found that the influence of hedgerows covering only 1%–5% of an area increased the effective roughness length by more than 50% in some cases.

6. Conclusions

Based on fair-weather daytime (unstable) data collected during IHOP_2002, the observed 10-m wind at the surface-flux sites is ~0.5–0.6 ± 0.2 m s^{-1} greater on average than modeled estimates found by applying MO similarity theory to data averaged along ~50–60-km flight legs. The track averages are based primarily on aircraft data collected at 65 m AGL. The differences increase by about 0.1 m s^{-1} when the estimated ~0.9-m displacement height is used. On individual days, particularly the uncertainty in momentum flux estimates leads to uncertainties as large as 0.4 m s^{-1}. Combining the days that fit the shear and MO similarity criteria using (7), the uncertainty is reduced to ~0.2 m s^{-1}.

The stronger observed winds result from the surface-flux station sites being chosen in open areas with z_0 of the order of a few centimeters; while the aircraft was taking measurements over and downstream not only of open fields, but also scattered buildings and trees, which bordered fields or were located along streams. These additional obstacles slowed the wind locally, and resulted in an effective roughness length for the Eastern Track of ~0.14 m based on data from 22 June, the day with the largest $-L$ and the least uncertainty. This z_0 value is significantly larger than the ~0.01–0.02-m values for the corresponding grassland flux sites 7–9.

The ~0.5–0.7 m s^{-1} discrepancy between NWP model and observed 10-m winds is comparable to the best model–observation comparisons reported by Zhang and Zheng (2004) and Liu et al. (2006). Because NWP models have grids with areas of order 1–100 km^2, the results imply that it is appropriate to compare surface winds derived from spatially averaged low-level aircraft data or take advantage of larger footprints represented by time-averaged data from taller towers (Hasager et al. 2003) or tethersondes for evaluation, rather than using averaged data from point 10-m measurements. In the absence of such data, the alternative for model evaluation is to allow for the fact that surface-site exposure can lead to measured winds stronger than representative of the area corresponding to a model grid using results from studies like this one.

Acknowledgments. Part of this work is extracted from D. Strassberg's senior thesis at the University of Colorado, Boulder. The NCAR portion of this research was supported by USWRP Grant NSF 01, NCAR Water Cycle Initiative, and the Advanced Study Program. We gratefully acknowledge the critical review by Bob Kelly of the University of Wyoming, Jielun Sun of NCAR, and two anonymous reviewers, whose comments significantly improved the manuscript. We also acknowledge the commitment, enthusiasm, and expertise of the Wyoming King Air aircrew and the National Center for Atmospheric Research staff in maintaining the surface-flux instruments, without which this work would not have been possible.

REFERENCES

Betts, A. K., R. L. Desjardins, and J. I. MacPherson, 1992: Budget analysis of the boundary layer grid flights during FIFE 1987. *J. Geophys. Res.,* **97,** 18 533–18 546.

Brock, F. V., and S. J. Richardson, 2001: *Meteorological Measurement Systems.* Oxford University Press, 290 pp.

Brutsaert, W., 1998: Land-surface water vapor and sensible heat flux: Spatial variability, homogeneity, and measurement scales. *Water Resour. Res.,* **34,** 2433–2442.

Businger, J. A., J. C. Wyngaard, Y. Izumi, and E. F. Bradley, 1971: Flux-profile relationships in the atmospheric surface layer. *J. Atmos. Sci.,* **28,** 181–189.

Campbell, G. S., and J. M. Norman, 1998: *Introduction to Environmental Biophysics.* 2nd ed. Springer, 286 pp.

Conzemius, R. J., and E. Fedorovich, 2006: Dynamics of sheared convective boundary layer entrainment. Part I: Methodological background and large-eddy simulations. *J. Atmos. Sci.,* **63,** 1151–1178.

de Rooy, W. C., and K. Kok, 2004: A combined physical–statistical approach for the downscaling of model wind speed. *Wea. Forecasting,* **19,** 485–495.

Desjardins, R. L., P. H. Schuepp, J. I. MacPherson, and D. J. Buckley, 1992: Spatial and temporal variations of the fluxes of carbon dioxide and sensible and latent heat over the FIFE site. *J. Geophys. Res.,* **97,** 18 467–18 475.

Glickman, T., Ed., 2000: *Glossary of Meteorology.* 2nd ed. Amer. Meteor. Soc., 855 pp.

Hasager, C. B., N. W. Nielsen, N. O. Jensen, E. Boegh, J. H. Christensen, E. Dellwik, and H. Soegaard, 2003: Effective roughness calculated from satellite-derived land cover maps and hedge-information used in a weather forecasting model. *Bound.-Layer Meteor.,* **109,** 227–254.

Kaimal, J. C., and J. J. Finnigan, 1994: *Atmospheric Boundary Layer Flows: Their Structure and Measurement.* Oxford University Press, 289 pp.

Kustas, W. P., J. H. Prueger, J. I. MacPherson, M. Wolde, and F. Li, 2005: Effects of land use and meteorological conditions on local and regional momentum transport and roughness for midwestern cropping systems. *J. Hydrometeor.,* **6,** 825–839.

LeMone, M. A., and Coauthors, 2007a: NCAR/CU surface, soil, and vegetation observations during the International H_2O Project 2002 field campaign. *Bull. Amer. Meteor. Soc.,* **88,** 65–81.

——, F. Chen, J. G. Alfieri, M. Tewari, B. Geerts, Q. Miao, R. L. Grossman, and R. L. Coulter, 2007b: Influence of land cover and soil moisture on the horizontal distribution of sensible and latent heat fluxes in southeast Kansas during IHOP_2002 and CASES-97. *J. Hydrometeor.,* **8,** 68–87.

Lenschow, D. H., 1995: Micrometeorological techniques for measuring biosphere–atmosphere trace gas exchange. *Biogenic Trace Gases: Measuring Emissions from Soil and Water,* P. A. Matson and R. C. Harriss, Eds., Blackwell Science, 126–163.

——, J. C. Wyngaard, and W. T. Pennell, 1980: Mean-field and second-moment budgets in a baroclinic, convective boundary layer. *J. Atmos. Sci.,* **37,** 1313–1326.

Liu, Y., F. Chen, T. Warner, and J. Basara, 2006: Verification of a mesoscale data-assimilation and forecasting system for the Oklahoma City area during the Joint Urban 2003 field project. *J. Appl. Meteor. Climatol.,* **45,** 912–929.

Mahrt, L., 2000: Surface heterogeneity and vertical structure of the boundary layer. *Bound.-Layer Meteor.,* **96,** 33–62.

Mann, J., and D. H. Lenschow, 1994: Errors in airborne flux measurements. *J. Geophys. Res.,* **99,** 14 519–14 526.

Moeng, C.-H., and P. P. Sullivan, 1994: A comparison of shear- and buoyancy-driven planetary boundary layer flows. *J. Atmos. Sci.,* **51,** 999–1022.

Paulson, C. A., 1970: The mathematical representation of wind speed and temperature profiles in the unstable atmospheric surface layer. *J. Appl. Meteor.,* **9,** 857–861.

Rife, D. L., C. A. Davis, Y. Liu, and T. Warner, 2004: Predictability of low-level winds by mesoscale meteorological models. *Mon. Wea. Rev.,* **132,** 2553–2569.

Schotanus, P., F. T. M. Nieuwstadt, and H. A. R. De Bruin, 1983: Temperature measurement with a sonic anemometer and its application to heat and moisture fluxes. *Bound.-Layer Meteor.,* **26,** 81–93.

Stull, R. B., 2000: *Meteorology for Scientists and Engineers.* Brooks/Cole, 502 pp.

Weckwerth, T. M., and Coauthors, 2004: An overview of the International H_2O Project (IHOP_2002) and some preliminary highlights. *Bull. Amer. Meteor. Soc.,* **85,** 253–277.

Wood, N., and P. Mason, 1991: The influence of static stability on the effective roughness lengths for momentum and heat transfer. *Quart. J. Roy. Meteor. Soc.,* **117,** 1025–1056.

Wyngaard, J. C., 1983: Lectures on the planetary boundary layer. *Mesoscale Meteorology—Theories, Observations, and Models,* D. K. Lilly and T. Gal-Chen, Eds., Reidel, 603–650.

Zhang, D.-L., and W.-Z. Zheng, 2004: Diurnal cycles of surface winds and temperatures as simulated by five boundary layer parameterizations. *J. Appl. Meteor.,* **43,** 157–169.